FAULT DIAGNOSIS OF GENERATION IV NUCLEAR HTGR COMPONENTS USING THE ENTHALPY-ENTROPY GRAPH APPROACH

C. P. du Rand* and G. van Schoor**

** School of Electrical, Electronic, and Computer Engineering, North-West University, Potchefstroom Campus, Private Bag X6001, Potchefstroom, 2520, South Africa E-mail: charl.durand@nwu.ac.za*
*** Unit for Energy Systems, North-West University, Potchefstroom Campus, Private Bag X6001, Potchefstroom, 2520, South Africa E-mail: george.vanschoor@nwu.ac.za*

Abstract: Fault diagnosis (FD) is an important component in modern nuclear power plant (NPP) supervision to improve safety, reliability, and availability. In this regard, a significant amount of experience has been gained in FD of generation II and III water-cooled nuclear energy systems through active research. However, new energy conversion methodologies as well as advances in reactor and component technology support the study of different FD methods in modern NPPs. This paper presents the application of the enthalpy-entropy (*h*-*s*) graph for FD of generation IV nuclear high temperature gas-cooled reactor (HTGR) components. The *h*-*s* graph is adapted for fault signature generation by comparing actual operating plant graphs with reference models. Multiple input feature sets (patterns) are generated for the fault classification algorithm based on the error, area, and direction of the fault residuals. The effectiveness of the FD method is demonstrated by classifying 24 non-critical single faults in the main power system of the Pebble Bed Modular Reactor (PBMR) during normal steady state operation as well as load following of the plant. Reference and fault data are calculated for the thermo-hydraulic network by means of a simulation model in Flownex® Nuclear. The results show that the proposed FD method produces different uncorrelated fault signatures for all the examined fault conditions.

Keywords: Fault diagnosis, enthalpy-entropy (*h*-*s*), high temperature gas-cooled reactor (HTGR), Pebble Bed Modular Reactor (PBMR), nuclear power plant (NPP).

1. INTRODUCTION

High levels of safety, reliability, and availability are challenging technology goals in the development of the next-generation nuclear power plants (NPPs) [1]. Accurate fault diagnosis (FD) plays an important role in these safety-critical systems providing crucial information regarding component health [2]. This work considers the fourth generation nuclear high temperature gas-cooled reactor (HTGR) energy system, with thermo-hydraulic models such as the Gas Turbine-Modular High Temperature Reactor (GT-MHR), and the Pebble Bed Modular Reactor (PBMR).

FD in NPPs comprises the fault isolation and identification tasks, and can be classified into methods that either utilise model-based or process history based (data-driven) techniques [2] - [4]. Model-based methods require an explicit mathematical system model and knowledge about the domain as well as the relationships between the different patterns of fault evolution. In practice, model-based methods are difficult to implement for systems with complex nonlinear dynamics such as NPPs, and are therefore mostly limited to linear applications or linear model approximations [2], [5]. Data-driven methods on the other hand, develop models from historical input-output process measurements, and require high quality (calibrated) and volume training data [2], [6]. These techniques are extensively studied for application in current water-cooled NPPs owing to the availability of system data and knowledge [2], [7 - 11]. Ma et al. [2] presents a complete review of current model-based and data-driven FD methods for monitoring different subsystems in NPPs.

Transients in NPPs can be initiated by component failure or malfunction [2], [11]. During a transient period, plant measurements develop unique patterns that differ from normal operating conditions. To date, artificial neural networks (ANNs) are the mostly studied algorithm for pattern classification in NPPs [2], [11]. However, practical applications in NPPs are still limited [2]. The main disadvantages of ANNs are their "black-box" structure (they do not offer justification or reasoning for their output), inflexibility regarding network adjustments (retraining needed), and the high volume of training samples required. Given these challenges, this research adapts the enthalpy-entropy (*h*-*s*) graph originally employed for analysis of a process's thermodynamic cycle to facilitate FD of new HTGR components. The application of this method inherently provides a transparent classification model that can be physically interpreted (i.e. heat transfer and work of different thermo-hydraulic sub-processes) while supervising only a minimum number of system variables. Furthermore, the proposed approach does not require large quantities of historical plant data for model development or retraining of the entire network for changes in reference parameters.

FD via the *h-s* graph approach is accomplished by comparing the actual operating *h-s* graph with a reference graph model. Changes in the shape of the supervised graph are therefore associated with specific component malfunctions. Representative fault signatures (patterns) are generated via multiple ensembles named the error and area error methods. Classifiers with multiple input feature sets obtained via different feature extraction methods normally exhibit complementary classification behaviour [12]. The application of the proposed FD approach is demonstrated by classifying 24 non-critical component faults in the PBMR during normal steady state operation as well as load following of the plant.

2. THE FAULT DIAGNOSIS APPROACH

2.1 Description of the HTGR

The HTGR under investigation, the PBMR, is a fourth generation nuclear energy system concept that employs a single-shaft, closed-loop direct Brayton thermodynamic cycle with helium gas as the primary coolant. This energy conversion methodology offers several advantages over traditional water nuclear reactor systems concerning operation, safety, and economics [13].

The HTGR design parameters allow for a maximum pressure of 9 MPa, reactor inlet and outlet temperatures of 500 °C and 900 °C respectively, and a 165 MWe output for a 400 MWt input. Figure 1 depicts the power cycle and the interconnection of the different main power system (MPS) components. The figure shows the gas flow path through the MPS and the eight thermo-hydraulic sub-processes.

The power output of the MPS is manipulated by regulating the gas inventory via the pressure differential between the MPS and the inventory control system (ICS). By using only the ICS, maximum cycle efficiency is achieved at all power levels for normal power operation [14].

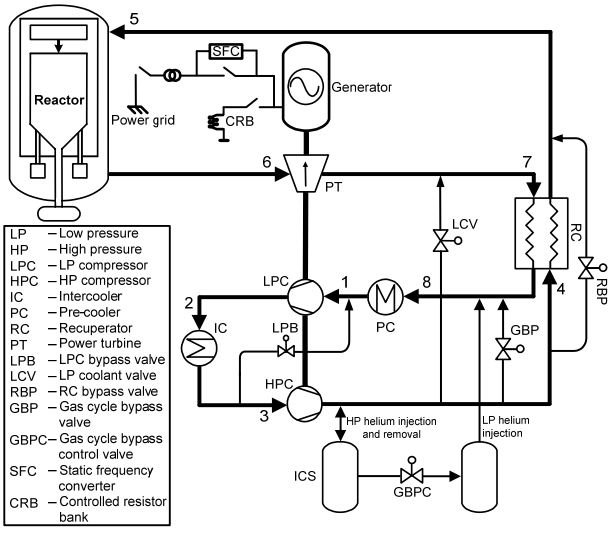

Figure 1: Schematic layout of the MPS.

2.2 Analysis of the HTGR thermodynamic cycle

Normal irreversibilities in the thermodynamic cycle, such as fluid friction, pressure losses, heat leakage, and non-isentropic compression and expansion losses, are best described using an *h-s* graph. The properties *h* and *s* facilitate a "non-black-box" fault classification structure that is physically interpretable. The property *h* describes the system's internal energy as well as the energy that is required to start fluid flow. The change in *h* for helium gas is defined as [15]

$$\Delta h = h_2 - h_1 = c_p \left(T_2 - T_1 \right) \tag{1}$$

with c_p and T the constant pressure specific heat (temperature independent) and temperature respectively.

The property *s* signifies the amount of internal energy that is not converted into work, and is applied to calculate the theoretical limits of energy conversion. The change in specific *s* is given by [16]

$$\Delta s = s_2 - s_1 = c_p \ln \frac{T_2}{T_1} - R \ln \frac{P_2}{P_1} \tag{2}$$

where *T*, *R*, and *P* denote the temperature, gas constant, and pressure respectively.

Normal system irreversibility alters the characteristics of the ideal cycle and accordingly, changes the shape of the *h-s* graph. Therefore, if the normal system irreversibility is known (practical cycle), discrepancies can be identified in the actual operating cycle. Plant transients cause the actual cycle graph to deviate from the reference graph model, thus producing residuals (errors) for *h* and *s*. The residuals are then used to generate different fault signatures (patterns) that correspond to the specific component malfunction. Figure 2 illustrates the proposed FD approach graphically. The node numbers in the figure correspond to the different sub-processes in the power cycle.

The primary power control mechanism of the HTGR under investigation produces a reference *h-s* graph model that remains relatively constant over the range of normal power operation. Therefore, different operating points are described with only one reference model. Figure 3 shows the practical cycle of the PBMR on a *T-P* and *h-s* graph for minimum and maximum continuous rating (MCR).

2.3 The error enthalpy-entropy method

The first FD method utilises the residual errors between the reference and actual operating *h-s* graphs to generate fault signatures

$$fs\left(i\right) = \frac{x_{ref}\left(i\right) - x_{actual}\left(i\right)}{x_{ref}\left(i\right)} \quad i = 1, 2, \ldots, n \tag{3}$$

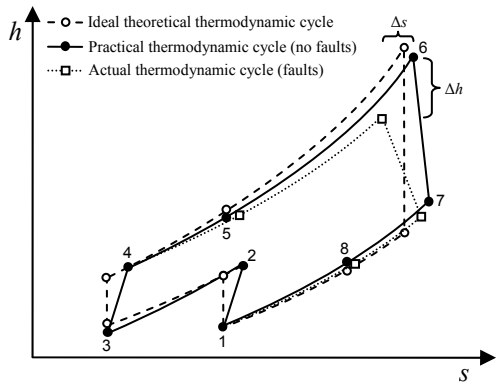

Figure 2: Fault diagnosis using the *h*-*s* graph.

with x denoting either h or s respectively, $x_{ref}(i)$ the reference node value, $x_{actual}(i)$ the actual node value, and i the node number (Figure 2). The actual and reference s are calculated independently by assigning reference values in (2) to T_1 and P_1.

However, (3) produces uncorrelated fault signatures for dynamic fault conditions. Accordingly, the h and s signatures are normalised to obtain graphic patterns that are independent from the fault magnitude. The normalised signatures are described by

$$fs_{norm}(i) = \frac{fs(i)}{\max_{i=1}^{n} |fs(i)|} \quad i = 1, 2, \ldots, n \tag{4}$$

with max $|fs(i)|$ the maximum value for all the nodes.

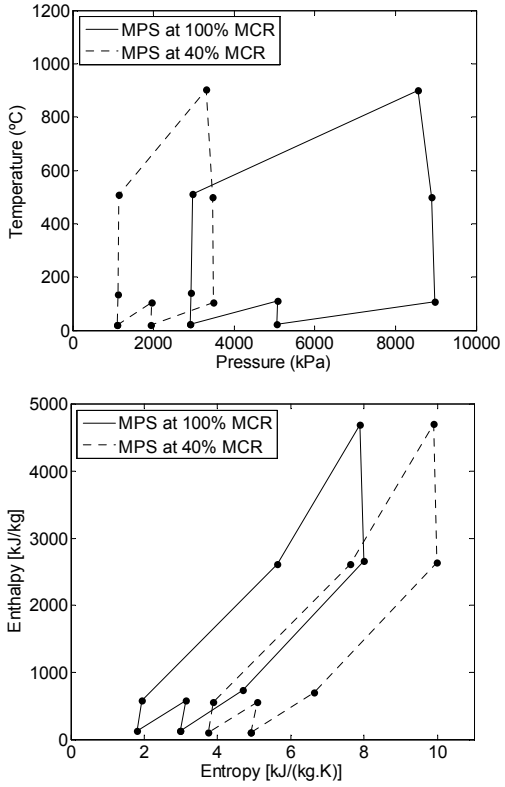

Figure 3: *T*-*P* and *h*-*s* graphs of the thermodynamic cycle.

Figure 4 presents an example of the normalised h and s signatures of a turbine pressure ratio fault for various fault magnitudes (percentage of maximum). The figure shows that the signatures are highly correlated with regard to fault direction and magnitude. Therefore, dynamic fault symptoms are described with one normalised h and s reference signature. This characteristic reduces the fault database to a minimum.

2.4 The area error enthalpy-entropy method

The second FD method utilises the area and direction of the residual shift between the reference and the actual operating *h*-*s* graphs to generate signatures. On each graph, two consecutive nodes (i) and (i + 1) are employed to describe the residual shift by means of a 2-dimensional boundary area. Figure 5 shows a graphical illustration of this signature generation method.

The distance between two graph nodes is given by [17]

$$r(d) = \sqrt{\left|h_j(k) - h_l(m)\right|^2 + \left|s_j(k) - s_l(m)\right|^2} \tag{5}$$

where j, l signify the reference a or fault b graphs, and k, m denote nodes i or (i + 1). Equation (5) is computed for nodes that are on the same or different graphs by setting $j = l$ or $k = m$ respectively. The residual area is then described according to the following fault graph variations:

1. the area is an irregular quadrilateral if the fault directions of nodes (i) and (i + 1) are the same (e.g. area 1 in Figure 5);
2. the area is triangular if only one fault node shifts (e.g. area 4 in Figure 5); and
3. the total area is given by the sum of two triangular areas if the fault directions of nodes (i) and (i + 1) differ (e.g. area 3 in Figure 5).

For the first variation, the area is determined by dividing the bounded segment into two triangular areas via a diagonal [18]. In the third variation, an intermediate value is defined at the graphs' crossover point to establish two individual triangular areas.

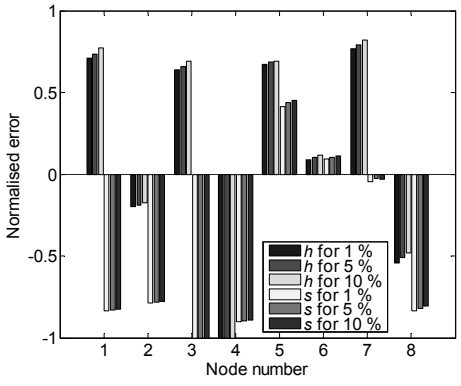

Figure 4: Normalised h and s error signatures for a decrease in turbine pressure ratio fault.

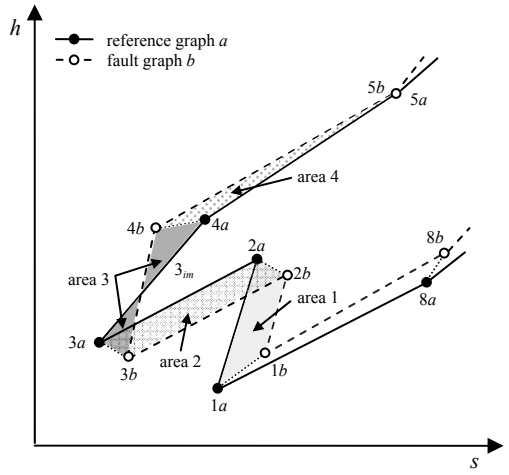

Figure 5: Description of the residual area errors between the reference and actual *h*-*s* graphs.

In the first method, different *h* and *s* signatures can be derived since (3) is calculated independently for each property. However, the residual areas derived via the area error method jointly summarise the shift in *h* and *s*. Therefore, to generate independent *h* and *s* signatures, separate fault directions are defined for *h* and *s* at fault node (*i*). Next, the *h* and *s* fault directions are multiplied with the corresponding residual area. The *h* and *s* area error fault signatures $fs_{area}(i)$ are computed using

$$fs_{area}(i) = \left[\sum_{1}^{q}\left(\sqrt{s_p\left(s_p - x\right)\left(s_p - y\right)\left(s_p - z\right)}\right)\right].dir(i) \tag{6}$$

with s_p the semiperimeter of each triangular area, x, y, and z the triangle side lengths, q the number of triangular areas, and dir (*i*) the *h* or *s* fault direction at node (*i*) (i.e. positive or negative).

Similar to (4), (6) is normalised to obtain signatures that are independent from the fault magnitude. Figure 6 shows the normalised *h* and *s* area error signatures for the turbine pressure ratio fault. If compared to Figure 4, it can be seen that different uncorrelated *h* and *s* signatures describe the component malfunction. The results therefore demonstrate that different fault feature sets can be extracted for the classification procedure via the *h*-*s* error and area error methods respectively.

3. APPLICATION OF THE FAULT DIAGNOSIS APPROACH

3.1 Modelling the HTGR

The MPS shown in Figure 1 is modelled using Flownex® Nuclear [19]. The main advantage of using Flownex® is that transient simulations are supported as well as advanced nuclear reactor models. Figure 7 shows the thermo-hydraulic model as a component network. The operating point of the model is manipulated by controlling the reactor outlet temperature (ROT), the pressure in the high pressure manifold (via the ICS), and the bypass valves. The system parameters for normal power operation at 100 % MCR are: ROT 900 °C, manifold pressure 9 MPa, compressor bypass valves fully closed, and the turbine-compressor shaft speed 6000 r/min (generator synchronised to power grid). Injection and extraction of helium gas are limited by a maximum ramp rate during MPS power output control. The *T* and *P* signals are monitored at the inlet nodes of the eight sub-processes to compute (1) and (2).

3.2 Categorisation of the HTGR fault classes

Three classes of component faults are identified via simplified cycle analyses of a three-shaft HTGR [20, 21]. The parameters and range of variation also attempt to describe many system uncertainties, originating from design, manufacturing, measuring, control, etc. The fault classes comprise variations in:

1. leak flows of the primary working fluid;
2. pressure losses in the primary circuit; and
3. component effectiveness or efficiency.

Leakage flows between system nodes are emulated using a resistive element with discharge coefficient (represents a throttling process) [19]. The secondary loss coefficients (*k*) of the inlet pipe models are changed to vary the pressure losses around the primary circuit. The heat transfer area between the hot and cold streams is decreased to reduce the effectiveness of the heat exchangers. The performance characteristics of the turbo machinery are varied by scaling the pressure ratio and efficiency as functions of corrected mass flow rate for various speed curves [19].

This study considers 24 non-critical single faults in the HTGR MPS that mainly influence the thermodynamic performance of the plant. The resulting fault transients are characterised by incipient time behaviour (small fault perturbation) and will therefore not initiate a PCU trip or reactor SCRAM (emergency shutdown of reactor). Table 1 presents a summary of the 24 single faults.

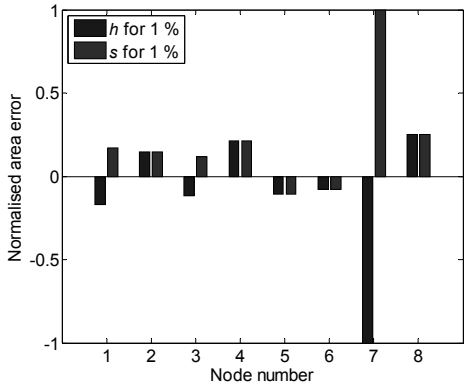

Figure 6: Normalised *h* and *s* area error signatures for a decrease in turbine pressure ratio fault.

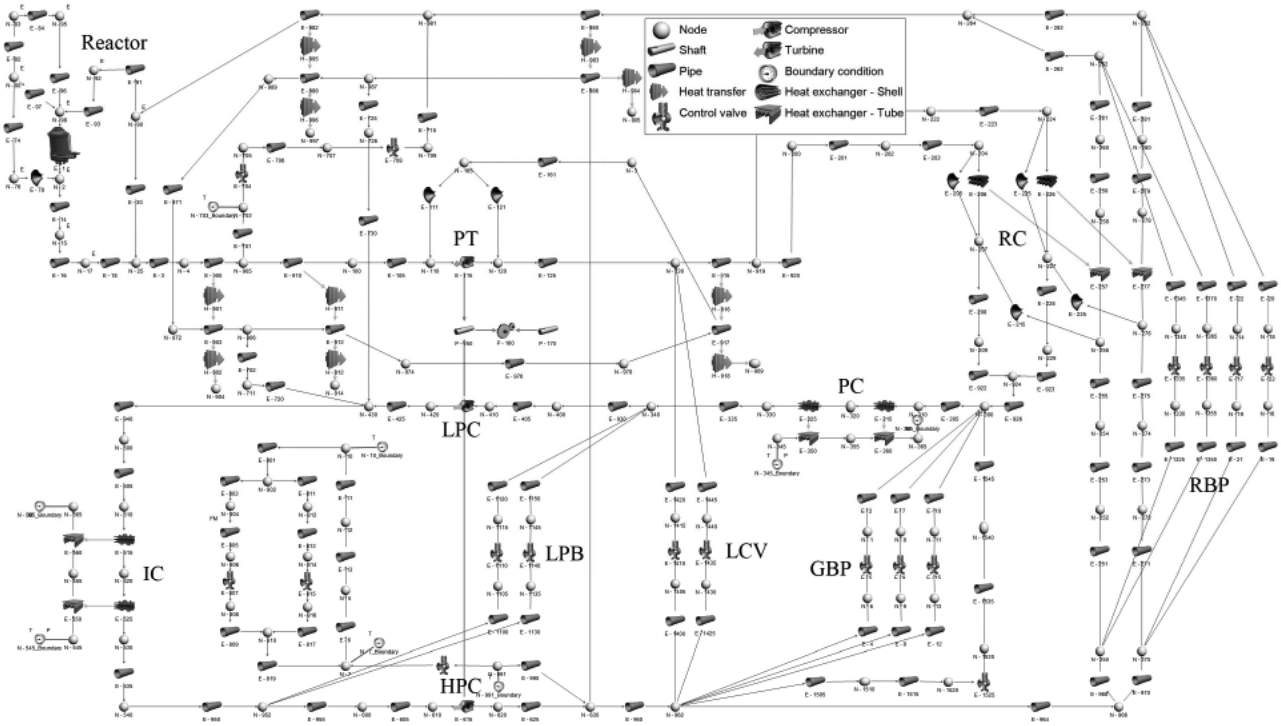

Figure 7: The Flownex® simulation model of the MPS.

Table 1: Summary of the single faults in the MPS

Description	Direction	Fault parameter
1. Pre-cooler heat transfer area	Decrease	a (m^2)
2. Intercooler heat transfer area	Decrease	a (m^2)
3. Recuperator heat transfer area	Decrease	a (m^2)
4. Recuperator HP to LP leakage	Increase	a (m^2)
5. LPC pressure ratio	Increase	scaling factor
6. LPC pressure ratio	Decrease	scaling factor
7. LPC efficiency	Decrease	scaling factor
8. HPC pressure ratio	Increase	scaling factor
9. HPC pressure ratio	Decrease	scaling factor
10. HPC efficiency	Decrease	scaling factor
11. Turbine pressure ratio	Increase	scaling factor
12. Turbine pressure ratio	Decrease	scaling factor
13. Turbine efficiency	Decrease	scaling factor
14. HP manifold leakage to outlet	Increase	a (m^2)
15. HP manifold leakage to inlet	Increase	a (m^2)
16. LPC inlet pipe losses	Increase	k
17. Intercooler inlet pipe losses	Increase	k
18. HPC inlet pipe losses	Increase	k
19. Recuperator HP inlet pipe losses	Increase	k
20. Reactor inlet pipe losses	Increase	k
21. Turbine inlet pipe losses	Increase	k
22. Recuperator LP inlet pipe losses	Increase	k
23. Pre-cooler inlet pipe losses	Increase	k
24. Reactor core bypass leakage	Increase	a (m^2)

3.3 Fault signature generation

Normal steady-state operation of the MPS at 100 % MCR is utilised to model the reference fault-free system. The fault transients are modelled individually as abrupt faults with a 1 % bias value. A small fault perturbation is chosen to demonstrate early FD of incipient faults. Since this work is mainly concerned with fault classification, it is assumed that the fault detection system recognises the onset of a component malfunction. As an example, Figure 8 depicts the signatures of different single faults. The figure shows that the correlation between the signatures is small for both signature generation methods regarding the nodes' residual magnitude and direction.

FD is important during load following of the plant to classify probable dynamic fault conditions. In this example, the following control characteristics are applied to manipulate the steady state operating point:

1. helium is injected and removed at a rate of 7.5 kg/s from the MPS via the ICS;
2. ROT is controlled at 900 °C via the control rods; and
3. GBPC valves are partially opened and closed.

Variations of the steady state reference graph model are utilised to facilitate GBPC valve operation. The results suggest that although GBPC valve operation changes the shape of the reference graph, the altered models remain relatively constant over the range of normal power operation. The fault transients evolve by way of an incipient time pattern (drift) representing a dynamic fault condition. A maximum fault magnitude of 2 % is reached at t = 4000 s. In practice, the examined fault symptoms will develop slowly over time. However, the fault evolution rate is increased to prevent lengthy simulations.

Figure 9 shows the signatures of fault 18 during load following of the MPS. The figure shows that the correlation between the signatures is good for both signature generation methods. The results show that static

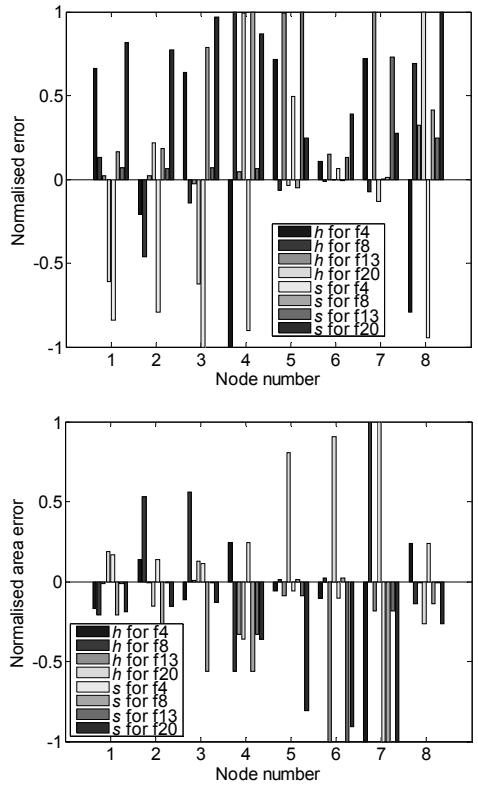

Figure 8: Normalised error and area error fault signatures for different fault classes.

signatures can describe dynamic fault conditions during normal power operation of the MPS, therefore reducing the size of the fault database.

4. CONCLUSION

This paper presented the *h-s* graph approach for FD of generation IV nuclear HTGR components. The *h-s* graph is implemented for fault isolation and identification, and aims to generate fault signatures (patterns) that are representative of NPP component malfunctions. The application of the proposed approach not only provides a transparent classification model (outputs can be interpreted), but also a flexible structure for model adjustment (e.g. retraining of entire model not required for changes in reference fault conditions).

FD is realised by comparing the actual operating cycle *h-s* graph with a reference graph model that includes normal system irreversibilities. Deviations from the practical cycle graph are associated with specific component malfunctions and used to generate different fault feature sets based on the error, area, and direction of the residual. An inventory power control mechanism produces a practical reference graph model that remains relatively constant over the range of normal power operation, which greatly simplifies the computational complexity of the fault diagnostic system. Accordingly, one reference model as well as single fault signatures facilitate FD of various component faults in different sub-processes of the MPS.

Steady state as well as dynamic Flownex® simulations indicate that all the examined faults can be described with uncorrelated signatures for variations of the normal process. The results show that the proposed approach successfully extracts different fault characteristics via the *h-s* graph, which can provide a robust FD solution in generation IV HTGRs. Continued research will be focused on applications in different thermo-hydraulic systems.

5. REFERENCES

[1] U.S. DOE Nuclear Energy Research Advisory Committee (NERAC) and the Generation IV International Forum (GIF): *A Technology Roadmap for Generation IV Nuclear Energy Systems*, Report no. GIF-002-00, December 2002.

[2] J. Ma and J. Jiang: "Applications of fault detection and diagnosis methods in nuclear power plants: A review", *Progress in Nuclear Energy*, Vol. 53 No. 3, pp. 255-266, April 2011.

[3] V. Venkatasubramanian, R. Rengaswamy, K. Yin and S.N. Kavuri: "A review of process fault detection and diagnosis - Parts I, II, III", *Computers and Chemical Engineering*, Vol. 27 No. 3, pp. 293-346, March 2003.

[4] M.D. Shah: "Fault detection and diagnosis in nuclear power plant - A brief introduction", *IEEE Conference on Engineering - Current Trends in Technology (NUiCONE)*, India, pp. 1-5, December 2011.

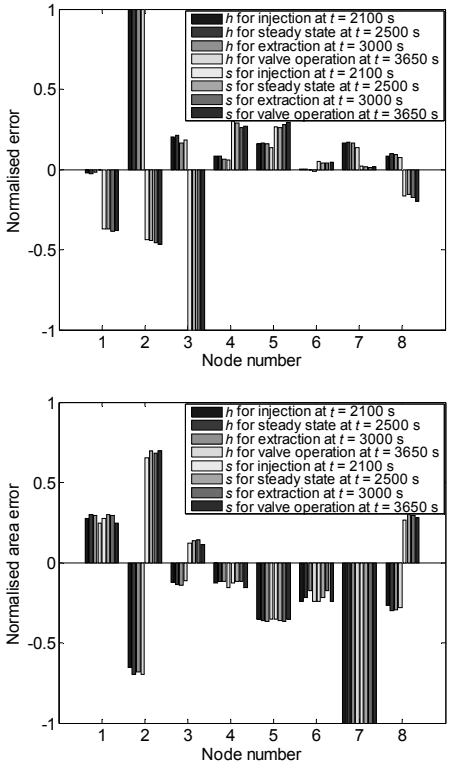

Figure 9: Normalised error and area error fault signatures of fault 18 during variations of the normal process.

[5] A. Evsukoff and S. Gentil: "Recurrent neuro-fuzzy system for fault detection and isolation in nuclear reactors", *Advanced Engineering Informatics*, Vol. 19 No. 1, pp. 55-66, January 2005.

[6] E. Zio, F. Di Maio and M. Stasi: "A data-driven approach for predicting failure scenarios in nuclear systems", *Annals of Nuclear Energy*, Vol. 37 No. 4, pp. 482-491, April 2010.

[7] B. Lu and B.R. Upadhyaya: "Monitoring and fault diagnosis of the steam generator system of a nuclear power plant using data-driven modelling and residual space analysis", *Annals of Nuclear Energy*, Vol. 32 No. 9, pp. 897-912, June 2005.

[8] C.M. Rocco and E. Zio: "A support vector machine integrated system for the classification of operation anomalies in nuclear components and systems", *Reliability Engineering and System Safety*, Vol. 92 No. 5, pp. 593-600, May 2007.

[9] B.R. Upadhyaya and K. Zhao: "Adaptive fuzzy inference causal graph approach to fault detection and isolation of field devices in nuclear power plants", *Progress in Nuclear Energy*, Vol. 46 No. 3-4, pp. 226-240, August 2005.

[10] E. Zio and G. Gola: "Neuro-fuzzy pattern classification for faults diagnosis in nuclear components", *Annals of Nuclear Energy*, Vol. 33 No. 5, pp. 415-426, March 2006.

[11] T.V. Santosh, G. Vinod, R.K. Saraf, A.K. Ghosh, and H.S. Kushwaha: "Application of artificial neural networks to nuclear power plant transient diagnosis", *Reliability Engineering and System Safety*, Vol. 92 No. 10, pp. 1468-1472, October 2007.

[12] Y. Lei, Z. He, Y. Zi and Q. Hu: "Fault diagnosis of rotating machinery based on multiple ANFIS combination with GAs", *Mechanical Systems and Signal Processing*, Vol. 21 No. 5, pp. 2280–2294, July 2007.

[13] P.G. Rousseau and G.P. Greyvenstein: "Changing the face of nuclear power via the innovative Pebble Bed Modular Reactor", *Proceedings: Power Generation World*, South Africa, pp. 1-22, March 2004.

[14] C. Nieuwoudt: *Demonstration plants operations summary*, PBMR (Pty) Ltd., Revision 4, South Africa, November 2002.

[15] A. Bejan and A.D. Kraus: *Heat transfer handbook*, John Wiley & Sons, Inc., New Jersey, p. 111, June 2003.

[16] A. Bejan: *Entropy generation minimization*, CRC Press, Florida, pp. 1-16, 205-231, October 1995.

[17] L.F. Costa and R.M. Cesar: *Shape analysis and classification: Theory and practice*, CRC Press, second edition, Boca Raton Florida, April 2009.

[18] C.B. Clapham: *Arithmetic for engineers*, Clapham Press, 2007.

[19] Flownex®: *General User & Library user manuals*, Version SE Nuclear, M-Tech Industrial, South Africa, 2009.

[20] P.G. Rousseau, G.P. Greyvenstein, B.W. Botha and C.G. Du Toit: "Sensitivity analysis of the PBMR gas cooled nuclear reactor cycle with the aid of a simplified simulation model", *IFAC Conference on Technology Transfer in Developing Countries*, South Africa, pp. 1-5, July 2000.

[21] E. Van Der Linde: "Evaluating the PBMR main power system turbo machines with the aid of sensitivity and Monte Carlo analyses", *Proceedings: 2nd International Topical Meeting on High Temperature Reactor Technology*, China, Paper D09, pp. 1-11, September 2004.